THE JOURNAL OF PHYSICAL CHEMISTRY B

ARTICLE

pubs.acs.org/JPCB

Longitudinal Zipping/Unzipping of Self-Assembled Organic Tubes

Xuejun Zhang, Tanmay Bera, Wenlang Liang, and Jiyu Fang*

Advanced Materials Processing and Analysis Center, Department of Mechanical, Materials and Aerospace Engineering, University of Central Florida, Orlando, Florida 32816, United States

ABSTRACT: Stimuli-responsive organic tubes are an attractive supramolecular assembly which has potential applications as a controlled release vehicle. We synthesize a smart organic tube by the coassembly of lithocholic acid (LCA) and taurolithocholic acid (TLCA) in aqueous solution. The coassembled LCA/TLCA tubes can be longitudinally unzipped into flat sheets by capillary force after being dehydrated on substrates. Consequently, the encapsulated guest molecules are released from the unzipping tubes. After the release of guest molecules, the flat sheets can be zipped back into hollow tubes upon hydration with aqueous solution. The zipping/unzipping LCA/TLCA tubes provide a new type of delivery vehicles, which may have potential for surface decontaminations.

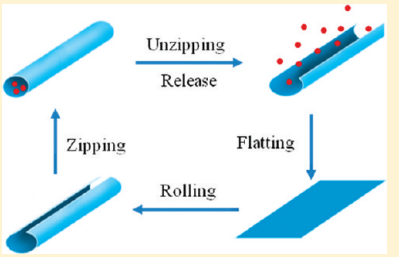

INTRODUCTION

Self-assembled organic tubes represent a potentially useful supramolecular structure that can be formed from amphiphilic molecules such as lipids and surfactants in solution.[1−4] They provide biological friendly aqueous confinements for encapsulating guest molecules.[5−12] It has been shown that the biomolecules confined inside self-assembled organic tubes are able to maintain their respective native activities.[6−8] There has been considerable interest in exploiting the application of self-assembled organic tubes as controlled release vehicles for drug delivery.[5,6,11,12]

Bile acids are biologically active surfactants.[13] The structure of bile acids is different from that of conventional surfactants. They have a hydrophilic concave side and a hydrophobic convex side rather than a long hydrophobic tail and a hydrophilic headgroup of conventional surfactants. The unique structure of bile acids and their derivatives is manifested in their unusual self-assembly behaviors in solution for synthesizing technically useful supramolecular structures such as micelles,[14] helical fibers,[15] lamellar sheets,[16] helical ribbons,[17−19] and hollow tubes.[20,21]

Stimuli-responsive organic tubes are attractive delivery vehicles, which allow us to control the release of encapsulated guest molecules.[22−26] It has been shown that the self-assembly behavior of lithocholic acid (LCA) (a secondary bile acid) is very sensitive to the condition under which self-assembly occurs.[24,25,27−31] Here we report a smart organic tube formed by the coassembly of lithocholic acid (LCA) and taurolithocholic acid (TLCA) in aqueous solution. The LCA/TLCA tubes can be unzipped along the longitudinal direction into flat sheets by capillary force after being dehydrated on substrates. As a consequence, the encapsulated guest molecules are released. Upon hydration with aqueous solution, the flat sheets roll up and zip into tubes. The potential application of the zipping/unzipping organic tubes is briefly discussed.

EXPERIMENTAL SECTION

Lithocholic acid (LCA) and taurolithocholic acid (TLCA) were obtained from Aldrich. The coassembly of LCA and TLCA

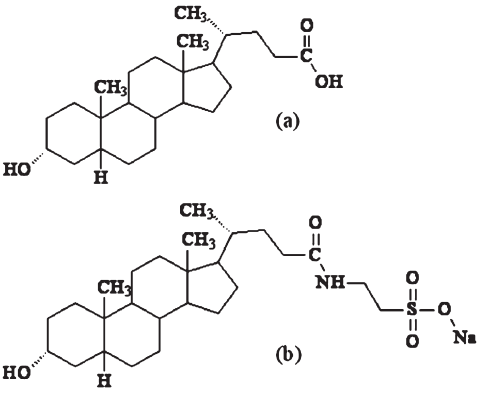

Figure 1. Chemical structures of LCA (a) and TLCA (b).

was carried out in aqueous solution with pH 8.0 in which the LCA and TCLA were first dissolved in sodium hydroxide (NaOH) solution and water, respectively. The two freshly prepared solutions were then mixed in room temperature. Loading of red dye 40 (disodium 6-hydroxy-5-((2-methoxy-5-methyl-4-sulfophenyl)azo)-2-naphthalene-sulfonate) into LCA/TLCA tubes was achieved by incubating the tubes with an aqueous solution containing the dye molecules at a concentration of ~0.1 mM for 24 h at room temperature for equilibration.

The self-assembled structures of LCA, TLCA, and LCA/TLCA mixtures were imaged with an Olympus BX40 microscope equipped with a digital camera (Olympus C2020 Zoom) in aqueous solution and an atomic force microscope (Dimension 3100, Veeco Instruments) on glass substrates. The size of silicon nitride cantilevers with a spring constant of 0.051 N/m was about 15 nm according to the manufacturer. Differential scanning calorimetry (DSC) studies were performed with a Seiko Instruments

Received: July 7, 2011
Revised: August 19, 2011
Published: November 10, 2011

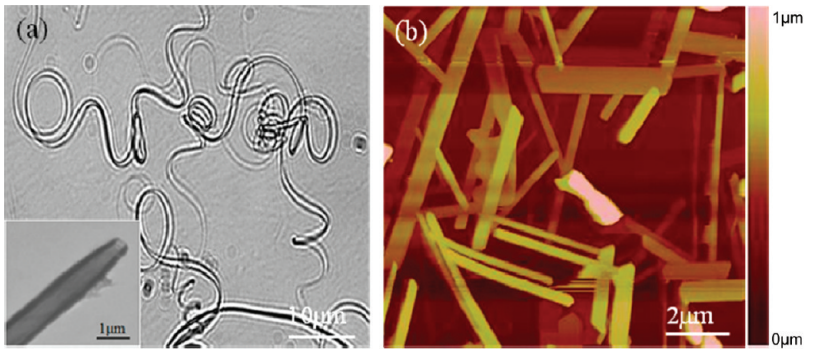

Figure 2. (a) Optical microscopy image of self-assembled LCA tubes in solution. TEM image of a dried LCA tube near its end was inset in a. (b) AFM image of self-assembled TLCA sheets on a glass substrate.

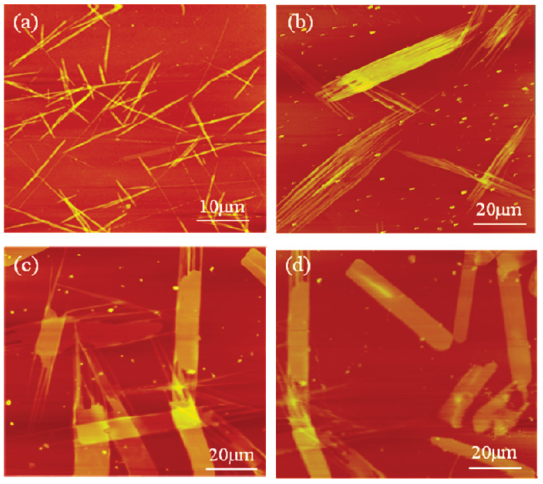

Figure 3. AFM images of self-assembled structures from LCA/TLCA mixed solution with a molar ratio of 0.2 after 2 (a), 6 (b), 10 (c), and 12 (d) days. These self-assembled structures were dried on glass substrates and then imaged in air at room temperature.

DSC100 differential scanning calorimeter. Tube solution (10 μL) was sealed in a DSC pan and then transferred to the calorimeter. The sample was scanned in the range from 20 to 80 °C at a heating rate of 5 °C/min. Scanning electron microscopy (SEM) measurements were carried out with a Zeiss Ultra-55 SEM operating at an acceleration voltage of 100 kV. Transmission electron microscopy (TEM) was performed with a JEOL JEM100SX-EM microscope operating at an acceleration voltage of 100 kV. The point compression on the LCA/TLCA tubes was carried out using a tungsten probe tip with a diameter of ~2 μm. The probe tip was controlled by a micropositioner (Signatone).

RESULTS AND DISCUSSION

Chemical structures of LCA and TLCA are shown in Figure 1. Our previous work showed that the LCA in sodium hydroxide (NaOH) solution with pH 12.0 self-assembled into spiral tubes by the linear aggregation of initially formed vesicles.[24] The mechanism of self-assembled LCA tubes differs from the mechanism of self-assembled lipid tubes in which the initially formed helical ribbons are a precursor.[32−35] The spiral LCA tubes with diameters in the range from 0.5 to 1.6 μm often collapse into a coil shape or contract into 2-D spirals after being dried on substrates (Figure 2a). However, the hollowness of dried LCA

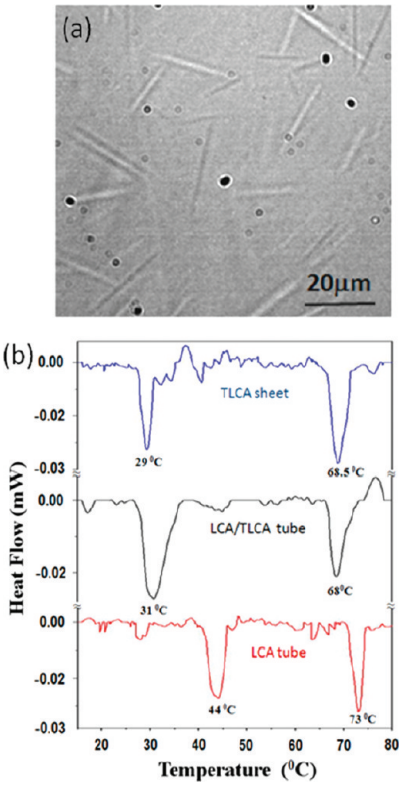

Figure 4. (a) Optical microscopy image of self-assembled LCA/TLCA tubes in solution. The tubes were formed in LCA/TLCA solution with a molar ratio of 0.2. (b) DSC thermograms of the LCA/TLCA tubes, LCA tubes, and TLCA sheet in solution.

tubes remains intact and is confirmed by the transmission electron microscopy (TEM) image inset in Figure 2a, which shows a contrast of electron density between the light central channel and the dark tube walls. The wall thickness of the LCA tube is about 110 nm. In contrast, the TLCA self-assembles into flat sheets with lengths in the range of 2−5 μm in water (Figure 2b). All the TLCA sheets have a smooth surface although their thicknesses and widths vary from one to another.

The coassembly of LCA and TLCA was carried out in aqueous solution with a pH of ~8.0 at room temperature. Briefly, LCA and TCLA were first dissolved in sodium hydroxide (NaOH) solution and water, respectively. The mixture of these two freshly prepared solutions was vortexed for 1 min. After being aged in a

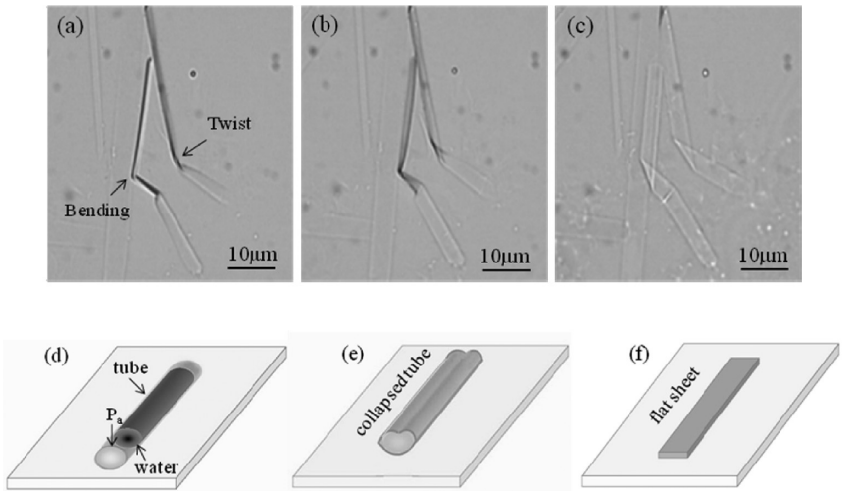

Figure 5. (a–c) Optical microscopy images of the longitudinal unzipping process of LCA/TLCA tubes after being dried on a glass substrate in air at room temperature. (d–f) Schematic process of unzipping a water-filled tube into a sheet on a substrate by the capillary pressure generated by a water meniscus inside the tube.

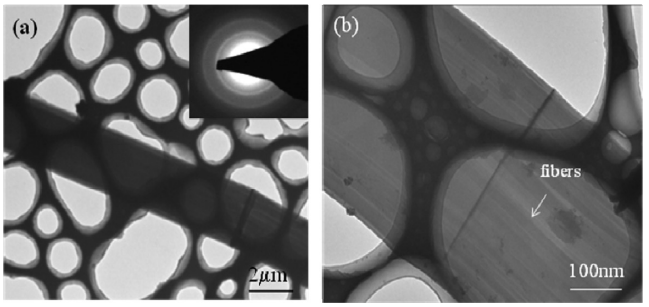

Figure 6. Low-resolution (a) and high-resolution (b) TEM images of flat LCA/TLCA sheets dried on carbon-coated grids. The electron diffraction was inset in (a).

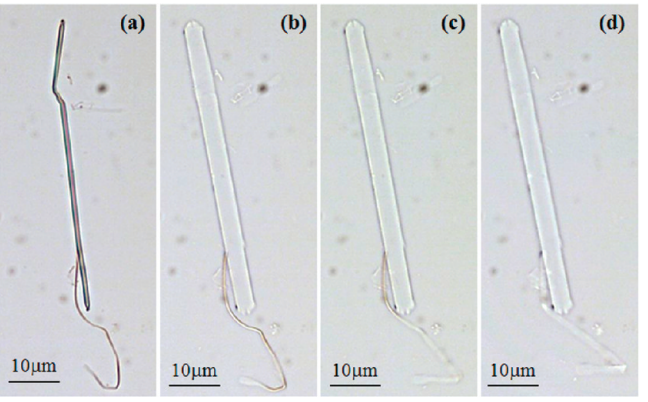

Figure 7. Optical microscopy images of the unzipping process of two red dye-loaded LCA/TLCA tubes with different diameters after being dried on a glass substrate. The images were taken at 0 s (a), 10 s (b), 20 s (c), and 30 s (d).

sealed glass vial for different time periods, the self-assembled structures from the mixed solution were dried on glass substrates and then imaged with an atomic force microscope (AFM) under tapping mode in air. The formation of fibers with a diameter of ~150 nm is observed after two days (Figure 3a). The initially formed fibers tend to laterally aggregate (Figure 3b) and fuse into sheets (Figures 3c and 3d) over time. After two weeks, the formation of tubes is observed in aqueous solution (Figure 4a). The mechanism of the sheet-to-tube transformation will be discussed in a later section. The average length of the tubes increases from 25 to 200 μm with the increase of LCA/TLCA molar ratio from 0.1 to 0.8. We carried out DSC measurements of LCA tubes, TLCA sheets, and LCA/TLCA tubes to measure their phase transition temperatures in solution. On heating, the LCA/TLCA tubes show two distinct endotherms with the phase transition temperatures at 30.8 and 68 °C, respectively (Figure 4b). The endotherm at 30.8 °C may be associated to the crystalline-to-fluid phase transition of LCA/TLCA tubes, while the endotherm at 69 °C represents the melting of the LCA/TLCA tubes. In situ optical microscopy measurements show that the morphology of LCA/TLCA tubes remains intact when they are heated to 30.8 °C. However, when the LCA/TLCA tubes are heated to 69 °C, we observe the complete melting of the LCA/TLCA tubes in solution. The LCA/TLCA tubes break into small particles. For comparison, the DSC thermograms of pure LCA tubes and pure TLCA sheets are also presented in Figure 4b. Both of them show two distinct endotherms. The phase transition temperature of TLCA sheets at 29 °C is lower than that of the LCA/TLCA tubes. The LCA tubes have a higher phase transition temperature (44 °C) and a melting temperature (73 °C), compared to the LCA/TLCA tubes. The difference in the phase transition temperatures between the mixed tube and the pure tube might reflect structural differences.

The LCA/TLCA tubes are able to transit into flat sheets after being dried on glass substrates. In situ optical microscope observations show that the transition is a result of the longitudinal unzipping of LCA/TLCA tubes. The unzipping begins near the ends of the tubes (Figure 5a) and then gradually extends along the longitudinal direction as the drying progresses (Figure 5b), leading to the formation of flat sheets (Figure 5c). The longitudinal unzipping can even go through the twisted and bent sites of LCA/TLCA tubes. The width of the flat sheet shown in Figure 5c is almost three times larger than that of the tube shown in Figure 5a, which agrees with the unzipping of a cylindrical tube into a flat sheet.

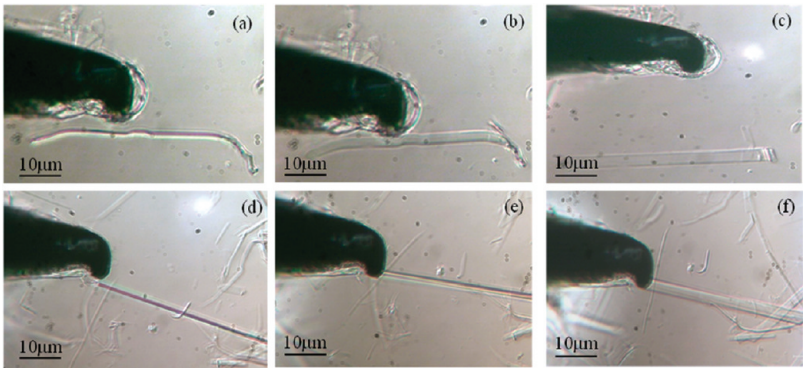

Figure 8. Optical microscopy images of unzipping dye-loaded LCA/TLCA tubes under local compressive forces. The local compressive force was applied on the middle section (a−c) and the end (d−f) of a dye-loaded tube. The tubes were formed in LCA/TLCA mixed solution with a molar ratio of 0.2.

It is known that the drying of water-filled tubes often causes them to collapse.[36−38] The collapse is a result of the capillary force induced by the formation of a water meniscus inside the tubes. The water meniscus is expected to first form near the ends of a drying tube (Figure 5d). The formation of the water meniscus will generate the effective pressure P_{eff} acting on the tube end, which can be estimated by the Laplace equation as follows:[38] $P_{eff} = (2\gamma \cos \theta)/(R)$, where γ is the surface tension of water, θ is the contact angle of water on the tube wall, and R is the tube radius. The critical pressure P_c for a tube to collapse can be estimated from the following formula for the stability of thin-walled tubes experiencing an outside pressure:[39] $P_c = (1/4)E(d/R)^3$, where E is the Young modulus of the tube, R is the tube radius, and d is the tube-wall thickness. If $P_{eff} > P_c$, the tube will collapse (Figure 5e). The deformation of the tube can generate a stress in the upper region of the tube wall. The observed longitudinal unzipping suggests that the stress generated by the deformation is sufficient to cleave the weak interactions along the longitudinal direction in the upper region of tube walls and unzip the tube into a sheet on the substrate (Figure 5f).

Figure 6a shows a low-resolution TEM image of a LCA/TLCA sheet dried on a carbon-coated grid. The sheet has a uniform width and two smooth edges along its length. The concentric rings of the electron diffraction (inset in Figure 6a) suggest that the sheet has a polycrystalline structure. The high-resolution TEM image shown in Figure 6b reveals that the LCA/TLCA sheet is made of parallel aligned fibers. Therefore, we infer that that the stress generated by the deformation cleaves the interactions of the parallel aligned fibers in the upper region of the tube walls. The capillary force-induced unzipping will first take place near the ends of a drying tube. As the evaporation is continuous, the water meniscus gradually moves to the middle region of the drying tube, which is in agreement with the longitudinal unzipping of LCA/TLCA tubes observed here.

To test the capability of the LCA/TCLA tubes for the encapsulation and release of guest molecules, we loaded red dye #40 into the tubes by adding them in a solution containing the dye molecules at a concentration of ∼0.1 mM. After incubation for 24 h for equilibration, a portion of the tube solution was diluted with dye-free aqueous solution. A drop of the diluted solution containing the dye-loaded tubes was placed on a glass substrate and then observed with an optical microscope in air at room temperature. The encapsulation and release of the red dye were monitored by simply observing the color change of the dye-loaded tubes with an optical microscope. As can been seen in Figure 7a, the dye-loaded tubes appear to be red. The homogeneity of the color suggests that the red dye molecules are relatively uniformly distributed inside the tubes. The color intensity remains unchanged until the tubes are unzipped (Figure 7b). The disappearance of the color indicates that the red dye molecules are released to the surrounding medium. In addition, we find that the unzipping of the small tube shown in Figure 7 is much slower than that of the large tube. The stepwise unzipping process starting from the end of the small tube is resolved (Figures 7c,d). The red dye molecules are gradually released as the stepwise unzipping of the small tube propagates. If we assume that the wall thickness d of the tubes is the same, we can infer that the tube with a large diameter unzips faster than the tube with a small diameter by comparing the effective pressure P_{eff} with the critical pressure P_c, which agrees with our observations. The width of the flat sheets shown in Figure 7d is almost three times larger than that of the zipped tubes shown in Figure 7a.

To further prove the unzipping of the LCA/TLCA tubes is triggered by mechanical stimuli, we applied a local pressure on the dye-loaded LCA/TLCA tubes with a tungsten probe tip. In our experiments, a dye-loaded tube with uniform red color was pushed down to a glass substrate in water by the probe tip under the guidance of an optical microscope (Figure 8a). As can be seen from Figure 8b, in response to the local compressive force which is applied on the middle section of the tube, the tube unzips into a flat sheet and releases the encapsulated dye molecules. Since the motion of the tungsten probe tip is controlled by a micropositioner, the exact applied force that is applied on the tube is unknown. After the probe tip is removed, the flat sheet remains on the substrate (Figure 8c). The dye-loaded tube can also be unzipped if the local compression is applied at its end (Figure 8d). It is clear that the tube collapses along the longitudinal direction under the local compressive force (Figure 8e) and then unzips into a flat sheet and releases the dye molecules (Figure 8f). It has been shown that under the local compression the generated stress in the upper region of the tube walls extends along the longitudinal direction.[40] The compression-induced stress along the longitudinal direction breaks the weak interactions of parallel aligned fibers in the upper region of LCA/TLCA tubes and causes them to unzip into flat sheets.

After the release of dye molecules, we hydrated the LCA/TLCA sheets dried on glass substrates by addition of aqueous solution. The hydrated sheets are found to detach from the glass surface and zip into tubes in aqueous solution (Figure 9). The transition from the LCA/TLCA sheets to tubes may be explained

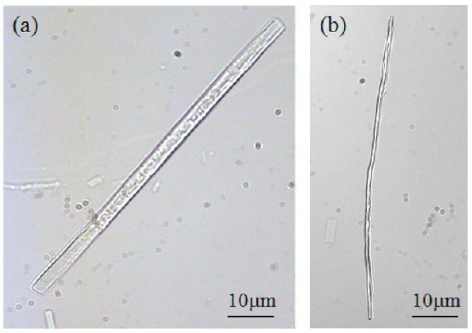

Figure 9. Optical microscopy images of the transition from an LCA/TLCA sheet (a) to a tube (b). The LCA/TLCA sheet dried on a glass substrate was hydrated by addition of aqueous solution on the substrate.

by the electrostatic polarization model proposed by de Gennes,[41] who points out that the symmetry in a chiral bilayer membrane allows the membrane to have a net electric dipole moment in the membrane plane. The electrostatic interaction between oppositely charged edges forces the membrane to roll up along the longitudinal direction and then zips into a tube.

In conclusion, we have presented here the assembly of LCA and TLCA into sheets, which spontaneously roll up and zip into tubular structures in aqueous solution. The unique feature of the self-assembled LCA/TLCA tubes is that they can be longitudinally unzipped into flat sheets after being dried on substrates. Consequently, the encapsulated guest molecules are released onto the substrates. After the release of guest molecules, the LCA/TLCA sheets zip back into tubes by the hydration with aqueous solution. The zipping/unzipping organic tubes represent a new type of delivery vehicles, which may have potential for the release of enzymes such as organophosphorous hydrolase for surface decontaminations. In the zipped form, the LCA/TLCA tubes with high aspect ratios provide protection for the encapsulated enzyme from the attack by denaturants' outside environments and suppress its unfolding for long-term storage purposes. When the enzyme is required for surface decontamination purposes, the dehydration-triggered unzipping of LCA/TLCA tubes on substrates will release the encapsulated enzyme to the substrate surface.

AUTHOR INFORMATION

Corresponding Author

*E-mail: jfang@mail.ucf.edu.

ACKNOWLEDGMENT

This work was supported by the National Science Foundation (CMMI-0726478 and CBET- 0855322).

REFERENCES

(1) Spector, M. S.; Selinger, J. V.; Schnur, J. M. *Materials-Chirality: Vol. 24 of Topics in Stereochemistry: Chiral molecular self-assembly*; Green, M. M., Nolte, R. J. M., Meijer, E. W., Ed.; Wiley: Hoboken, 2003.

(2) Shimizu, T.; Masuda, M.; Minamikawa, H. *Chem. Rev.* **2005**, *105*, 1401–1444.

(3) Brizard, A.; Oda, R.; Huc, I. *Top. Curr. Chem.* **2005**, *256*, 167–218.

(4) Fang, J. Y. *J. Mater. Chem.* **2007**, *17*, 3479–3484.

(5) Schnur, J. M.; Price, R. R.; Rudolph, A. S. *J. Controlled Release* **1994**, *28*, 3–13.

(6) Meilander, N. J.; Pasumarthy, M. K.; Kowalczyk, T. H.; Cooper, M. J.; Bellamkonda, R. V. *J. Controlled Release* **2003**, *88*, 321–331.

(7) Yu, L. T.; Banerjee, I. A.; Gao, X. Y.; Nuraje, N.; Matsui, H. *Bioconjugate Chem.* **2005**, *16*, 1484–1487.

(8) Kameta, N.; Masuda, M.; Minamikawa, H.; Mishima, Y.; Yamashita, I. M.; Shimizu, T. *Chem. Mater.* **2007**, *19*, 3553–3560.

(9) Zhao, Y.; Mahaja, N.; Fang, J. Y. *Small* **2006**, *2*, 364–367.

(10) Guo, L.; Chowdhury, P.; Fang, J. Y.; Gai, F. *J. Phys. Chem. B* **2007**, *111*, 14244–14249.

(11) Kameta, N.; Minamikawa, H.; Masuda, M.; Mizuno, G.; Shimizu, T. *Soft Matter* **2008**, *8*, 1681–1687.

(12) Kameta, N.; Minamikawa, H.; Someya, Y.; Yui, H.; Masuda, M.; Shimizu, T. *Chem.—Eur. J.* **2010**, *16*, 4217–4223.

(13) Mukhopadhyay, S.; Maitra, U. *Curr. Sci.* **2004**, *87*, 1666–1683.

(14) Venkatesan, P.; Cheng, Y.; Kahne, D. *J. Am. Chem. Soc.* **1994**, *116*, 6955–6956.

(15) Blow, D. M.; Rich, A. *J. Am. Chem. Soc.* **1960**, *82*, 3566–3571.

(16) Tellini, V. H. S.; Jover, A.; Galantini, L.; Pavel, N. V.; Meijide, F.; Tato., J. V. *J. Phys. Chem. B.* **2006**, *110*, 13679–13681.

(17) Zastavker, Y. V.; Asherie, N.; Lomakin, A.; Pande, J.; Donovan, J. M.; Schnur, J. M.; Benedek, G. B. *Proc. Natl. Acad. Sci. U.S.A.* **1999**, *96*, 7883–7887.

(18) Wang, X.; Lu, Y.; Duan, Y.; Meng, L.; Li, C. *Adv. Mater.* **2008**, *20*, 462–465.

(19) Qiao, Y.; Lin, Y.; Wang, Y.; Yang, Z; Liu, J.; Zhou, J.; Yan, Y.; Huang, J. *Nano Lett.* **2009**, *9*, 4500–4504.

(20) Tellini, V. H. S.; Jover, A.; Meijide, F.; Tato, J. V.; Galantini, L.; Pavel, N. V. *Adv. Mater.* **2007**, *19*, 1752–1756.

(21) Manghisi, N.; Leggio, C.; Jover, A.; Meijide, F.; Pavel, N. V.; Tellini, V. H. S.; Tato, J. V.; Agostino, R. G.; Galantini, L. *Angew. Chem., Int. Ed.* **2010**, *49*, 6604–6607.

(22) Abidian, M. R.; Kim, D. H.; Martin, D. C. *Adv. Mater.* **2006**, *18*, 405–409.

(23) Matsui, H.; Golongan, B. *J. Phys. Chem B* **2000**, *104*, 3383–3386.

(24) Zhang, X.; Zou, J.; Tamhane, K.; Kobzeff, F. F.; Fang, J. Y. *Small* **2010**, *6*, 217–220.

(25) Zhang, X. J.; Mathew., M.; Gesquiere, A. J.; Fang, J. Y. *J. Mater. Chem.* **2010**, *20*, 3716–3721.

(26) Kameta, N.; Tanaka, A.; Akiyama, H.; Minamikawa, H.; Masuda, M.; Shimizu, T. *Chem.—Eur. J.* **2011**, *19*, 5251–5255.

(27) Terech, P.; de Geyer, A.; Struth, B.; Talmon, Y. *Adv. Mater.* **2002**, *14*, 495–498.

(28) Terech, P.; Dourdain, S.; Bhat, S.; Maitra, U. *J. Phys. Chem. B* **2009**, *113*, 8252–8267.

(29) Pal, A.; Basit, H.; Sen, S.; Aswalb, V. K.; Bhattacharyax, S. *J. Mater. Chem.* **2009**, *19*, 4325–4334.

(30) Tamhane, K.; Zhang, X.; Zou, J.; Fang, J. Y. *Soft Matter* **2010**, *6*, 1224–1228.

(31) Zhang, X. J.; Fang, J. Y. *Soft Matter* **2010**, *6*, 2139–2142.

(32) Selinger, J. V.; Spector, M. S.; Schnur, J. M. *J. Phys. Chem. B* **2001**, *105*, 7157–7169.

(33) Spector, M. S.; Singh, A.; Messersmith, P. B.; Schnur, J. M. *Nano Lett.* **2001**, *1*, 375–378.

(34) John, G.; Masuda, M.; Okada, Y.; Yase, K.; Shimizu, T. *Adv. Mater.* **2001**, *13*, 715–718.

(35) Zhao, Y.; Mahajan, N.; Lu, R. B.; Fang, J. Y. *Proc. Natl. Acad. Sci. U.S.A.* **2005**, *102*, 7438–7442. Mahajan, N.; Zhao, Y.; Du, T. B.; Fang, J. Y. *Langmuir* **2006**, *22*, 1973–1976.

(36) Yu, M. F.; Kowalewski, T.; Ruoff, R. S. *Phys. Rev. Lett.* **2001**, *86*, 87–90.

(37) Mahajan, N.; Fang, J. Y. *Langmuir* **2005**, *21*, 3153–3157.

(38) Seleznev, V.; Yamaguchi, H.; Hirayama, Y.; Prinz, V. *Jpn. J. Appl. Phys.* **2003**, *42*, L791–L794.

(39) Landau, L. D.; Lifshitz, E. M. *Theory of Elasticity*, 3rd ed.; Pergamon Press: Oxford, 1986.

(40) Zhao, Y.; Tamhane, K.; Zhang, X.; An, L; Fang, J. Y. *ACS Nano* **2008**, *2*, 1466–1472.

(41) De Gennes., P. G. *C. R. Acad. Sci. Paris* **1987**, *304*, 259–263.